ACS OMEGA

Open Access

http://pubs.acs.org/journal/acsodf

Article

Highly Sensitive Potentiometric pH Sensor Based on Polyaniline Modified Carbon Fiber Cloth for Food and Pharmaceutical Applications

Md. Sanwar Hossain, Narayanasamy Padmanathan, Md. Mizanur R. Badal, Kafil M. Razeeb,* and Mamun Jamal*

Cite This: *ACS Omega* 2024, 9, 40122−40133

Read Online

ACCESS | Metrics & More | Article Recommendations | Supporting Information

ABSTRACT: This study introduces a potentiometric pH sensor that is extremely sensitive and specifically designed for food and pharmaceutical applications. The sensor utilizes a pH-sensitive interface fabricated by electropolymerizing polyaniline (PANI) on carbon fiber cloth (CFC). Structural and morphological analyses of PANI-CFC and CFC have been conducted by using X-ray diffraction (XRD), field emission scanning electron microscopy (FESEM), and X-ray photoelectron spectroscopy (XPS). The investigation of the functional groups was conducted by using Fourier transform infrared spectroscopy (FTIR) and Raman spectroscopy. The electrochemical characteristics were assessed by utilization of cyclic voltammetry (CV) and open-circuit potential (OCP) measurements in a three-electrode configuration. The sensor exhibited a sensitivity of 60.9 mV/pH, while retaining consistent performance within the pH range of 4 to 12. The repeatability and robustness of the sensors were verified. The accuracy of the PANI-CFC sensor was confirmed by validation using real samples, demonstrating its compatibility with commercially available pH sensors. The application of density functional theory (DFT) calculations revealed an interaction energy of −173.2886 kcal/mol, indicating a strong affinity of H^+ ions towards PANI-CFC electrode. Further investigation was conducted to examine the chemical reactivity of PANI, revealing a HOMO−LUMO energy gap of −0.98 eV. This study highlights the PANI-CFC sensor as a reliable and efficient pH-sensing platform for food and pharmaceuticals applications, performing robustly in both laboratory and real-world settings.

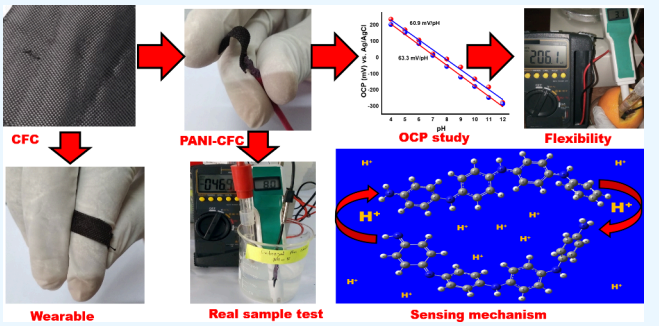

1. INTRODUCTION

The logarithmic concentration of hydrogen ions or pH acts as an important quantitative, diagnostic, and surrogate parameter in industrial, physiological, and clinical practices.[1,2] The pH sensor thus has a wide range of applications, such as food and beverage, environmental monitoring, chemical processing, biomedical applications (e.g., body fluid and blood analysis), and laboratory pH measurements.[3−7] The pH sensing techniques are based on various methods, such as potentiometric, capacitive, chemiresistive, luminescence, and optical methods.[8−11] Potentiometric pH sensors are the most popular because their size can be reduced, the device structure is simple, and the unit cost of fabrication is relatively low.[8,12] Improving the sensitivity is a key challenge in potentiometric pH sensors despite their advantages, such as ease of use and low cost. Highly sensitive sensing materials are essential for accurate measurements over a wide pH range. Thus, significant research efforts have been aimed at developing novel materials with enhanced sensitivity and stability.[13]

Several types of pH sensor have been developed to measure H^+ ion concentration.[14] Glass pH electrodes have been widely used for centuries because of their sensitivity, selectivity, and stability for measuring pH levels.[15] However, it is susceptible to damage from certain chemicals and its bulky size limits its application in microscale or implant testing. To overcome this issue, metal oxide-based materials, such as tungsten trioxide (WO_3), iridium dioxide (IrO_2), platinum dioxide (PtO_2), titanium oxide (TiO_2), and tin oxide (SnO_2), have been extensively investigated for their potential application in pH sensing.[16−20] These materials offer favorable properties for pH detection, including high chemical stability and tunable surface reactivity.[21−23] However, challenges, such as hysteresis, flexibility, and potential drift, have limited their widespread adoption, prompting researchers to explore alternative

Received: July 1, 2024
Revised: August 30, 2024
Accepted: September 2, 2024
Published: September 12, 2024

materials and approaches. To overcome these limitations, there is a need for smaller, more flexible, and biocompatible pH sensors suitable for various testing environments such as food and pharmaceutical applications.[24]

Conducting polymers, such as polyaniline (PANI), show great promise for pH sensing owing to their unique properties, such as environmental stability, affordability, and adjustable conductivity. In particular, PANI stands out for its resilience, low cost, ease of preparation, and reversible conductivity control through charge transfer doping and protonation, making it versatile for a wide range of applications.[23,24] Recently, Zhu *et al.* introduced a flexible pH sensor based on polyaniline modified oily polyurethane/polypropylene spunbonded nonwoven fabric. This 3D PANI pH sensor demonstrated good mechanical properties and Nernst response of −67.67 mV/pH.[25] Additionally, Kim *et al.* developed a polyaniline/graphene (PANI-Graphene) based sensor for real-time sweat monitoring on the human body, which exhibited a Nernstian sensitivity of 61.91 mV/pH.[26] Furthermore, Zea *et al.* developed a polyaniline/polypyrrole ink for a fully printed highly sensitive pH sensor for pharmaceutical applications.[25] This sensor showed excellent reproducibility with a linear super-Nernstian response (81.2 ± 0.5 mV/pH unit) in a wide pH range (pH 3−10). However, Cheng *et al.* developed a very flexible nanofiber pH sensor made by electrodepositing PANI on gold fibers.[27] With a response slope of 60.6 mV/pH in the pH range 4−8. Additionally, Lee *et al.* suggested a flexible paper-based PANI pH sensor with biodegradable and ultraflexible properties. This paper-based pH sensor exhibited high sensitivity (58 mV/pH in the pH range of 2−12).[28] Furthermore, Mahinnezhad *et al.* developed a fully printed potentiometric pH sensor using a polyaniline/graphite composite. The sensors were tested across a pH range of 3−10, demonstrating linear, stable, and near-Nernstian sensitivity of 53 mV/pH.[29] These developments highlight the potential of polyaniline-based pH sensors for flexible, affordable, and highly sensitive applications in various fields including food, pharmaceuticals, and environmental monitoring.

Carbon fiber cloth (CFC) has emerged as a promising substrate material for wearable pH sensors that require high mechanical strength, flexibility, and conductivity.[30−33] CFC offers excellent mechanical properties and a two-dimensional conducting framework that serves as an ideal support for conducting polymers such as PANI. The integration of PANI with CFC simplifies the electrode preparation process and enhances the overall performance of the flexible pH sensors. One advantage of these hybrid materials is that they do not require the addition of a binder or conductive agent during electrode preparation. However, few studies have focused exclusively on novel bare carbon fiber cloths. The development of conductive polymer-modified CFC as a flexible electrode is highly desirable for achieving high-performance pH-sensing systems.

In this study, we developed a novel approach for fabricating a PANI-modified CFC pH sensor with the aim of achieving exceptional sensitivity and Nernstian response across a wide pH range. We employed cyclic voltammetry to directly electropolymerize aniline onto the surface of the CFC, followed by a comprehensive characterization of the surface properties of the sensor using various spectroscopic techniques. The electrochemical experiments revealed the sensor's exceptional sensitivity and its ability to respond to variations in pH. The accuracy of the PANI-CFC sensor was confirmed by validation using real samples, such as vinegar, malta, and antacid. The sensor's measurements exhibited a high degree of correspondence with those obtained from a commercially available pH meter. This pH sensor is particularly remarkable, as it is capable of measuring changes in pH on the curved surface of malta even as it is bent, which is an application that cannot be achieved with the standard pH meters. Furthermore, we used density functional theory (DFT) calculations to study the electronic transport properties of PANI and elucidate its protonation and deprotonation dynamics. By integrating experimental and theoretical insights, along with characterization and real samples test, this study advances the frontier of flexible pH sensor technology with implications to food and pharmaceutical industries and beyond.

2. MATERIALS AND METHODS

2.1. Chemicals and Materials. E-Merck, Germany, provided aniline (C_6H_7N) (≥99.5% CAS: 62−53−3), sulfuric acid (H_2SO_4) (95−97%, CAS: 7664−93−9), and hydrochloric acid (HCl) (37%, CAS: 7647−01−0). Sodium dihydrogen phosphate (NaH_2PO_4) (ACS reagent, ≥98% CAS:10049-21-5), disodium hydrogen phosphate (Na_2HPO_4) (Reagent Plus®, ≥99.0%, CAS:7558-79-4), sodium bicarbonate ($NaHCO_3$) (ACS reagent, ≥99.7% CAS:144-55-8), and sodium carbonate (Na_2CO_3) (anhydrous soda (CAS Number: 497-19-8), and were purchased from Sigma-Aldrich (Germany). The conducting glue was supplied by ERCON (USA). Aniline (C_6H_7N) (ACS reagent, ≥99.5% CAS: 62-53-3) and CFC were purchased from Sigma-Aldrich. Copper conductor wire was purchased from Khulna Hardware. Beximco Pharmaceuticals in Bangladesh supplied Sarsons malt vinegar and Rennie antacid chewable tablets. Without change, the chemicals were of analytical grade and pure. The phosphate buffer solutions contained sodium phosphate salt, sodium hydroxide, and hydrochloric acid. The studies used ultrapure Millipore water with a resistivity of 18.2 MΩ.cm.

2.2. Fabrication of pH Sensor. In order to produce the electrode, a piece of CFC material was precisely cut into a size of 1 cm × 0.5 cm using a ruler. The rectangular CFC working electrode underwent a cleaning process using an intense 3 M hydrochloric acid. Silver conductive adhesive was utilized to establish a connection between the CFC and the copper wire, while an inert insulating polymer was employed to encase the connecting portion of the CFC electrode. Subsequently, the electrodes were cleansed with deionized water to eliminate any residual adhesives prior to electrochemical depositions. PANI-CFCs were produced by electrochemically polymerizing PANI in a three-electrode setup using the Biologics SP-300 potentiostat. The electrolyte solution was generated by combining a solution containing 0.1 M aniline with a solution containing 1.0 M H_2SO_4. The electropolymerization process was conducted via the cyclic voltammetry method, employing a potential range of −0.1 to 0.8 V for 10−16 cycles, with a scan rate of 10 mVs^{-1}. The PANI/CFC was subsequently rinsed multiple times with deionized water to eliminate any residual ionic compounds. It was then air-dried for a duration of 6 h at room temperature (Scheme 1).

2.3. Characterization. FT-IR spectra were obtained using the IRTracer-100 instrument manufactured by SHIMADZU. A Kratos AXIS ULTRA spectrometer was utilized to conduct X-ray photoelectron spectroscopy (XPS) analysis. Raman spectra

https://doi.org/10.1021/acsomega.4c06090
ACS Omega 2024, 9, 40122−40133

Scheme 1. Preparation of PANI-CFC Electrode and Application

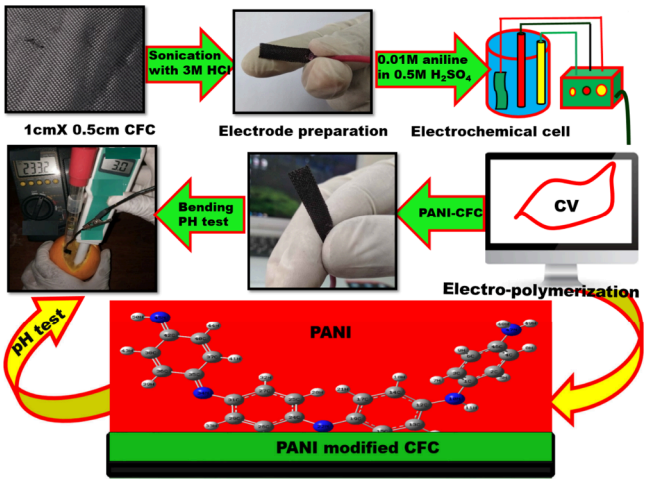

were acquired with a Renishaw (RA100) confocal Raman microscope with a 514.5 nm excitation laser wavelength. The composites' crystallinity was assessed using X-ray powder diffraction (XRD) with a Philips PW3710-MPD diffractometer equipped with an Oxford Instruments INCA energy system and Cu Kα radiation (λ = 1.54 Å). The film's morphology was examined using the FEI Quanta 650 field-emission scanning electron microscope (FE-SEM) equipped with an energy-dispersive X-ray spectroscopy (EDX) Oxford Instruments INCA energy system.

2.4. Electrochemical Experiment. An electrochemical study was conducted using a three-electrode cell. It contains platinum, Ag/AgCl, and PANI-CFC electrodes as the counter, reference, and working electrodes, respectively. The preparation of pH 4−12 solutions involved utilizing a 0.01 M solution of acetate, phosphate, and carbonate buffer. After each pH measurement, the CFC-PANI electrode was washed with deionized water. For the purpose of evaluating the performance and reusability of the sensor, a minimum of three repetitions were conducted for each data point during the data collection process. No deterioration was observed throughout the electrochemical measurement.

2.5. Computational Method. The computational calculations were performed using the Gaussian 16, Revision C.01 series of programs.[32] The DFT-PBEPBE/6-311+G (d, p) level of theory was used to compute the energy of geometries, Mullkin charge, and IR. However, the PANI structure was completely optimized using DFT-B3LYP/6-311+G (d, p) and Molecular orbital analysis (HOMO and LUMO).

3. RESULTS AND DISCUSSION

3.1. Fabrication and Morphology Characterization. Electrochemical polymerization of aniline has been carried out on the CFC electrode using cyclic voltammetry (CV) in aqueous solution containing 0.1 M aniline and 1 M H_2SO_4 (Figure 1a). Voltammogram reveals the growth and deposition of PANI through successive redox cycles. As depicted in Figure 1(a), the CV curve of PANI at a scan rate of 10 mVs^{-1} displays two distinct pairs of peaks (a, m), indicative of two reversible oxidation processes within the PANI membrane, illustrating excellent reversibility. During the forward scan, two significant redox peaks (a*, m*) are observed: the first peak corresponds to the conversion of the leucoemeraldine base to an intermediate emeraldine state, while the second peak indicates the transition from the intermediate state to the fully oxidized pernigraniline state (Supplementary Figure S1).[34,35] In the reverse scan, two reduction peaks appear, representing the reverse reaction of the oxidation processes.

In the first cycle, aniline monomers undergo oxidation, forming radical cations that begin to polymerize, marking the initiation of nucleation on the CFC surface (Figure 1b). As the number of cycles increases, the peak currents of both oxidation and reduction peaks within the range of −0.1 to 0.8 V progressively escalate, indicating the continuous growth and deposition of PANI on the CFC. Each cycle contributes to the layer-by-layer growth of PANI, with the peak currents increasing due to the accumulation of more polymer material on the electrode surface. The consistent appearance of redox peaks with each cycle signifies the excellent reversibility of the redox processes and the stability and flexibility of the PANI film (Supplementary Figure S2). Over successive cycles, polymerization leads to a uniform PANI coating on the CFC, resulting in a homogenized surface thickness. The measurement of tensile strength has been found 1.06 × 10^{-6} $N{\cdot}m^{-2}$ for the PANI modified surface with thickness of 45 μm,

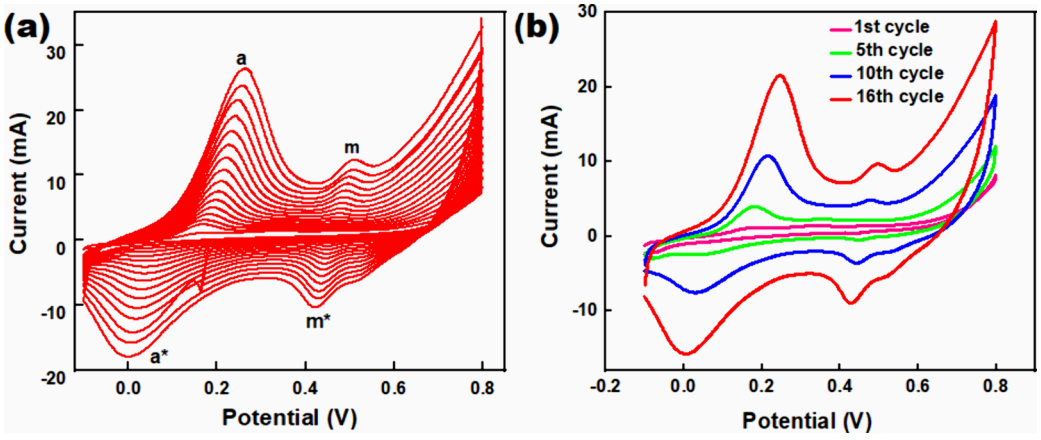

Figure 1. (a) Cyclic voltammogram (CV) of electropolymerization of polyaniline on CFC, and (b) CV summary of electropolymerization process on CFC (conditions: CFC working electrode, platinum wire counter electrode, and Ag/AgCl reference electrode, 0.1 M aniline in 1 M H_2SO_4 at scan rate 10 $mV.s^{-1}$, oxidizing agent 1 M H_2SO_4).

https://doi.org/10.1021/acsomega.4c06090
ACS Omega 2024, 9, 40122−40133

compare to blank CFC of 1.70×10^{-6} N·m^{-2} (UTM, Model 25ST, Tinius Olsen Ltd., UK). A continuous growth of polymer is evident in Figure 1b confirming the successful polymerization of aniline on the CFC electrode. The process begins with nucleation in the initial cycle, followed by growth and homogenization of the PANI layer in subsequent cycles, ultimately achieving a uniform PANI film on the CFC surface. Adhesive tape test has been done to examine the adhesion of the PANI film on CFC, and it has found strong adhesion. As polymerization has been done electrochemically and CFC is a porous material, the polymer made a stable film onto the CFC.

3.2. Field Emission Scanning Electron Microscopy (FESEM) Study with EDX. The surface morphology of CFC and PANI/CFC was studied using FESEM with EDX. Figure 2(a,b) displays FESEM images of the CFC at low and high magnifications, revealing the rod-like structure of the CFC with a diameter of 200 nm. The FESEM images of the PANI-modified carbon fiber cloth are illustrated in Figure 2(c–f) at various magnifications. It shows the initial stages of PANI growth on the carbon fiber, indicating a successful modification. The PANI-CFC FESEM images exhibit distinct nanowire structures with diameters ranging from 40 to 83 nm, as seen in Figure 2(e,f). The average diameter of the PANI nanowires was determined to be approximately 70.2 nm and thickness of PANI on CFC is 35–45 μm (Supplementary Figure S3). Additionally, a highly porous structure of PANI-CFC was observed. This porosity suggests potential benefits in sensing technology, where an increased surface area and enhanced reactivity are advantageous. Figure 2(d–f) shows a bulk quantity of uniformly grown nanowire structures on the carbon fiber surface, indicating a controlled synthesis of PANI nanowires on the carbon cloth fiber, enhancing its surface properties compared to the original CFC. The EDX images in Figure 2(g,h) conclusively verified the successful polymerization of aniline on the CFC, further supporting the presence of PANI on the modified surface. A thorough investigation via FESEM with EDX revealed a transformation in the surface morphology of the CFC, showcasing a distinct nanowire structure upon chemical modification with PANI. This controlled synthesis not only confirmed the successful polymerization of aniline on the CFC, but also highlighted promising applications in sensor technology, demonstrating enhanced surface properties for advanced technological utilization.

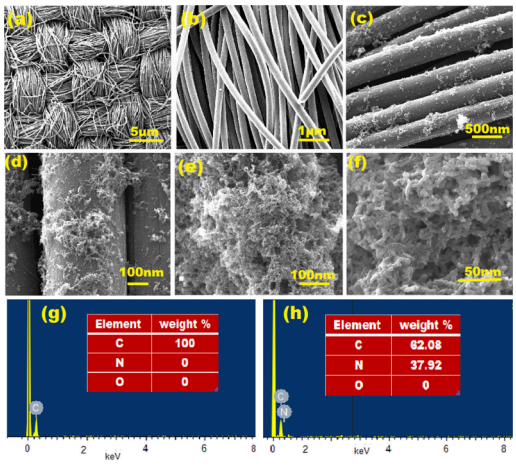

Figure 2. (a,b) SEM images of blank CFC with different magnification; (c,d) PANI-CFC after 10 cycles; (e,f) PANI-CFC after 16 cycles with different magnifications; and (g,h) EDX of CFC and PANI-CFC after 16 cycles with 0.1 M aniline.

3.3. Fourier Transformed Infrared (FTIR). The functional groups of the CFC and PANI-CFC were thoroughly investigated using Fourier-transform infrared (FTIR) spectroscopy, as illustrated in Figure 3a. The FT-IR spectrum of the PANI-based electrode exhibits several prominent peaks, which are indicative of its characteristic functional groups. Notably, the peak at 1546 cm^{-1} corresponds to the C═C stretching vibration of the quinoid ring, while the peak at 1475 cm^{-1} is associated with the C═C stretching of the benzenoid ring.[36] Additionally, the peak at 1301 cm^{-1} is attributed to CN stretching within the benzenoid units. The CN stretching vibration of the quinoid units appears at 1024 cm^{-1}, and the CH out-of-plane bending vibration is evident at 781 cm^{-1}, both of which are highlighted in Figure 3a.[37] Moreover, a notable band at 3714 cm^{-1} indicates the presence of hydrogen bonding within the PANI-CFC. This hydrogen bonding is crucial, as it can influence the overall stability and electrical properties of the material. Another significant peak at 2355 cm^{-1} corresponds to the stretching vibration band of two benzene nuclei.[21,38−40] These spectral features collectively demonstrate the intricate molecular architecture of the PANI-CFC composite, confirming the presence of key functional groups and interactions that contribute to its unique properties and potential applications in various fields, including electronics and materials science.

3.4. Raman Spectra Analysis. The Raman spectra of PANI were recorded using 514.5 nm excitation, as shown in Figure 3b. The bands observed in the wavenumber range of 1100−1700 cm^{-1} correspond to the stretching modes of various bonds. The Raman band at 1597 cm^{-1} is assigned to the C−C stretching vibration of the benzene ring. The band at 1561 cm^{-1} is attributed to N−H deformation vibrations. The band in the range of 1341−1352 cm^{-1} provides information about carrier vibrations in PANI, specifically in the C−N polaronic structure. The weak band at 1276 cm^{-1}, which is not marked in Figure 3b, can be assigned to the C−N stretching mode of the polaronic unit. The intense band observed at 1183 cm^{-1} is related to C−H vibrations of aromatic rings. The bands in the range of 1000 to 400 cm^{-1} provide information about the deformation vibrations of the benzene rings.[41−43] The spectra for CFC revealed two distinguishing bands at 1350 and 1586 cm^{-1}, known as the D and G bands, respectively.[41−43] The G band is associated with the tangential stretching vibrations of the C−C bonds, while the D band is derived from disordered structures or defects in the carbon.

3.5. X-ray Powder Diffraction (XRD). Figure 3c displays the XRD patterns of the CFC and PANI-CFC. The XRD spectrum of the CFC shows broad peaks in the range of 11.37−31.24°, indicative of its amorphous nature and (002) plane of CFC.[44] In contrast, the PANI exhibits characteristic peaks at 2θ = 15.08−43.80°, corresponding to the periodicity perpendicular and parallel to the polymer chain, respectively.[45,46] Additionally, the peak at 2θ = 25.08° (200) is attributed to the layered arrangement of polymer chains at alternating distances.[47] The XRD patterns of PANI-CFC display both the characteristic peaks of PANI and the broad peak of the CFC. This indicates that PANI has been successfully integrated into the CFC, maintaining its own crystalline structure while overlaying the amorphous background of the CFC.

https://doi.org/10.1021/acsomega.4c06090
ACS Omega 2024, 9, 40122−40133

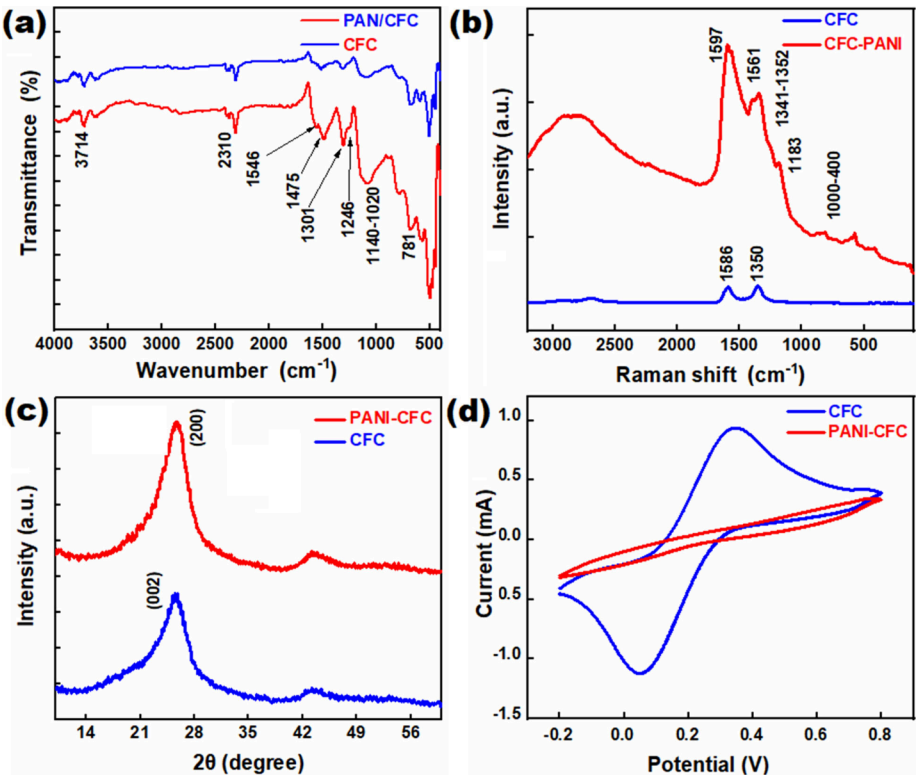

Figure 3. (a) FT-IR spectrum of PANI-CFC and CFC; (b) Raman spectrum; (c) XRD of PANI-CFC and unmodified CFC; and (d) CV of PANI-CFC and CFC.

3.6. CV Analysis of PANI-CFC and CFC. The growth of PANI on the CFC surface is further examined using CV profiles measured in standard 5 mM potassium ferricyanide and potassium ferrocyanide solutions, as illustrated in Figure 3d. The red and blue colors in Figure 3d represent the PANI-modified and unmodified electrodes, respectively. The CV curve for unmodified CFC exhibits prominent redox peaks, indicating active electrochemical reactions on the surface. In contrast, the PANI-CFC electrode does not show any surface redox reactions, which suggests that the surface is effectively coated with PANI. This absence of redox peaks in the PANI-modified electrode is indicative of the successful electrochemical polymerization of aniline on the CFC surface. Consequently, the electrochemical properties of the PANI-CFC are significantly altered compared to those of the unmodified CFC, demonstrating a successful modification process.

3.7. X-ray Photoelectron Spectroscopy (XPS) Analysis of CFC and PANI-CFC. XPS was studied to identify the presence of chemical composition and the oxidation state of specific elements in the samples. The survey spectrum peaks at 283.7, 399.1, 534.2, and 975.5 eV for PANI-CFC and CFC correspond to C 1s, N 1s, O 1s, and S 2p, respectively, as shown in Figure 4a. The core-level spectrum of C 1s in Figure 4b shows peaks at 284.6, 285.3, 286.4, and 287.3 eV. Figure 4b are attributed to C−C, C═N, C═NH^+, and C═O functionalities, respectively. The peak at 288.0 eV is characteristic of carbon connected to oxygen (C═O), indicating the presence of C−O functional groups in PANI.[48−54] The core-level spectra of N 1s in the PANI-CFC, shown in Figure 4c, deconvolute into three peaks at 400.1, 400.3, and 402.1 eV, corresponding to C−N, neutral/tertiary amine (C═N), and quaternary amine/protonated imine (C═NH^+), respectively, aligning closely with literature values.[55−59] Additionally, the core-level spectra of O 1s in PANI-CFC, shown in Figure 4d, reveals a peak at 531.8 eV, which represents C═O.[60−62] The peak at 532.0 eV is assigned to hydroxyl (C−OH) and ether (C−O−C) groups, while the peak at 533.1 eV corresponds to chemisorbed oxygen, water, or ethanol was used for washing after polymerization. The presence of the S 2p state in the electrode indicates the incorporation of SO_4^{2-} ions during the electrochemical deposition of PANI in the H_2SO_4 acid electrolyte bath (Figure 4e). Thus, XPS confirms the elemental composition and chemical structure of polymers on the CFC.

3.8. pH Sensitivity and Reproducibility. PANI-CFC electrodes were used to measure pH by calculating the open circuit potential (OCP) across a range of buffer solutions with pH values from 4 to 12, as shown in Figure 5a. The OCP results indicate that the PANI-CFC-based sensor exhibits excellent performance in detecting H^+ ions. Just for information, without PANI, CFC does not work as a pH sensor, which has been shown in Supplementary Figure S4. This is attributed to the presence of amino (−NH) groups in the polymeric structure of PANI. The pH value reflects the concentration of H^+ ions in a solution, which can be related to the oxidation−reduction potential according to the Nernst Equation (eq 1). Nernst Equations (eq 1), where E_0 is standard electrode potential, R is the molar gas constant, T is the absolute temperature, and F is the Faraday constant.

$$E_1 = E_0 + \frac{RT}{F}\ln[H^+]$$

$$E_1 = E_0 + 0.591 \log[H^+] \quad (1)$$

The potential difference was measured using a PANI-CFC electrode in 0.1 M phosphate-buffered solutions. The

https://doi.org/10.1021/acsomega.4c06090
ACS Omega 2024, 9, 40122−40133

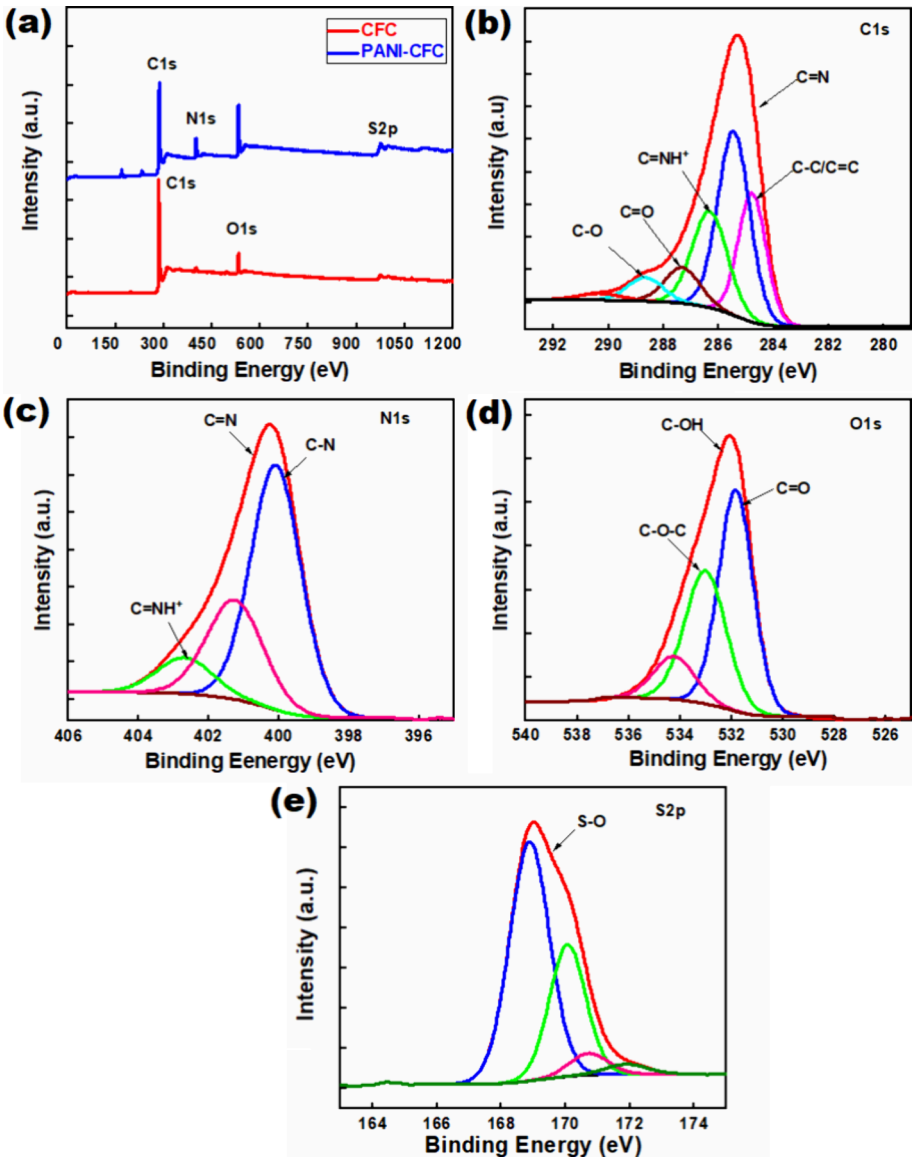

Figure 4. PANI-CFC and CFC materials: (a) survey spectrum; (b) C 1s spectra of PANI-CFC; (c) N 1s spectra of PANI-CFC; (d) O 1s spectra of PANI-CFC; and (e) S 2p spectra of PANI-CFC.

equilibrium potential was recorded across a pH range of 4 to 12. This approach allowed for the assessment of the electrode's response to varying H^+ ion concentrations, further demonstrating its effectiveness as a pH sensor.

The PANI-CFC electrode demonstrated the ability to determine pH with a sensitivity of 60.9 mV/pH (R^2 = 0.99), which is very close to the theoretical Nernst equation value of 59.2 mV/pH (Figure 5b). The potential difference was measured as a function of pH, showing a linear correlation across the pH range from 4 to 12 (Figure 5b). Reproducibility and potential drift were also assessed, with the results corresponding well to the Nernst equation in Figure 5(c,d). Compared with other available systems, no prior work has demonstrated the use of PANI-CFC as an environmentally friendly pH platform made of polymer materials. The reproducibility of two sensors is illustrated in Figure 5c, showing an absolute potential range for pH 4 to 12 and a sensitivity range of 60.9 to 63.3 mV/pH. Despite absolute potential fluctuations, these sensors exhibited a relative standard deviation (RSD, n = 5) in sensitivity of 2.3%, with an average sensitivity of 62.3 mV/pH (Supplementary Table S1). This indicates that the PANI-modified sensor has an excellent H^+ detection capability.

Interference, stability, and drift measurements of the PANI-CFC sensor were conducted and are shown in Supplementary Figure S5. OCP was measured for buffer solutions with pH values of 4, 6, 7, and 11 (representing mildly acidic, low acidic, neutral, and mildly basic conditions, respectively). Data were collected in each buffer solution for three h at 30 min intervals (Figure 5d). After 3 h, the potential drift in the neutral pH buffer was found to be 10 mV, while in acidic and basic media, the potential drifts were 200 mV (pH 4), 82 mV (pH 7), and −248 mV (pH 11). The largest drift was observed at pH 7, representing a deviation of 2.3% from the peak potential.

The stability of the sensor was further assessed over a continuous three-month period, during which it retained up to 98% of its initial sensitivity (Supplementary Figure S5d). After 3 h of continuous use, the sensor showed a potential drift of 1.97−2.33% and maintained 98% of its initial sensitivity after three months. In contrast, the CFC electrode alone (without

https://doi.org/10.1021/acsomega.4c06090
ACS Omega 2024, 9, 40122−40133

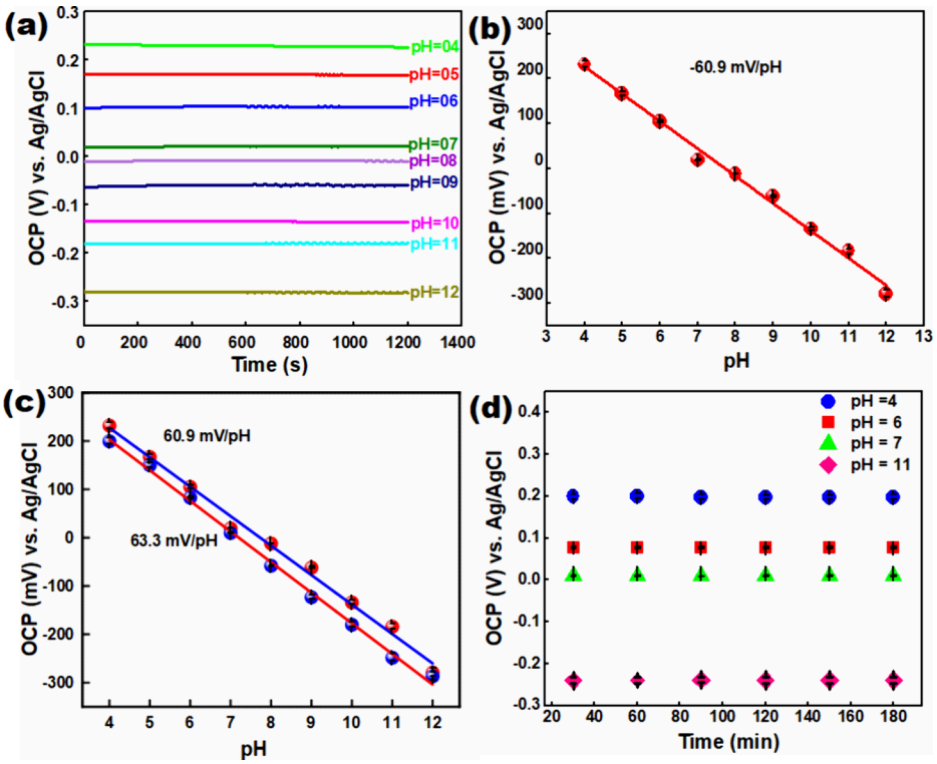

Figure 5. (a) Potential response of PANI-CFC at different pH (4−12) in 0.1 M buffer-solution; (b) the corresponding linear relation plot of pH (4−12); (c) reproducibility; and (d) potential drift test (electrode configuration: PANI-CFC working electrode, platinum wire counter electrode, and Ag/AgCl reference electrode).

PANI modification) was tested for pH response using a 0.1 M phosphate-buffered saline solution. It was found that the CFC electrode could not detect H^+ ions and did not display a linear response, indicating that it does not conform to the Nernst eq (Supplementary Figure S4). This highlights the critical role of PANI modification in enabling effective pH detection.

3.9. Interference and Temperature Effects. The effect of interfering ions was determined by adding different concentrations (10 μM to 15 mM) of interfering ions (NH_4Cl, $CaCl_2$, NaCl, $Na_2(SO_4)$, $ZnSO_4$, and $MgCl_2$), which are shown in Supplementary Figure S5(a). The output potential change for increasing concentrations of the interfering ions is calculated by taking into account the change at each stage. The maximum distortion response was found with the addition of 15 mM $MgCl_2$, due to the reaction of the high concentration of $MgCl_2$ with water ingredients, which results in the production of $Mg(OH)_2$, acting as a strong base and significantly changing the pH of the solution. In addition, the accuracy of pH measurement is required to study the effect of temperature on the sensitivity, repeatability, and physical properties of the PANI-CFC electrode. Usually, the mobility of ions increases with the increasing the temperature of the solution, but viscosity decreases. Furthermore, the dissociation of weak acids and bases increases with increasing temperature, which means the concentration of H^+ changes in the solution. The effect of temperature was studied and measured for the OCP vs temperature start from 15 to 50 °C, as depicted for pH 4, 7, and 10 in Supplementary Figure S5b), and found pH increases with temperature. The temperature coefficient values of 3.0, 2.5, and 3.0 mV with corresponding pH values of 4, 7, and 10 were observed.

A comparative study of polyaniline (PANI)-based pH sensors involves evaluating their performance characteristics, such as sensitivity, stability, and selectivity, in comparison to other pH sensing materials or even different configurations of PANI-based sensors, as shown in Table 1.

Table 1. Electrochemical Performance of Different Potentiometric pH Sensors

Sensing material	pH range	Sensitivity (mV/pH)	Reference
OPU/PP SF	2.0−8.0	67.67	25
3D PANI	4.0−9.0	69.33	63
PANI and polypyrrole	3.0−10.0	81.20	64
PANI membrane	5.4−8.6	58.57	2
polyaniline	3.9−10.1	62.40	12
PANI-Gr	2.0−13.0	61.91	26
PANI/Graphite	3.0−10.0	53.00	29
MoS_2-polyaniline	4.0−8.0	70.40	29
PANI-CFC	4.0−12.0	60.90	This work

3.10. Real Sample Test. Real sample tests of vinegar, antacid plus, and Malta are illustrated in Figure 6(a−c), where the PANI-CFC working electrode and the Ag/AgCl reference electrode were connected to a multimeter. PANI-CFC electrode was dipped into the Malta, along with the reference electrode, and a commercial pH meter. PANI-CFC electrode was tested both in straight and bending conditions (Figure 6c). The potential difference was found to be 203.4 mV, which is equivalent to a pH of 3.4. The commercial pH meter also shows a pH of 3.1. The OCP measurements using the PANI-CFC sensor indicated pH values of 2.4 for Malta, 5.1 for vinegar, and 8.9 for the antacid solution (Figure 6d). For comparison, the commercially available glass pH sensor

https://doi.org/10.1021/acsomega.4c06090
ACS Omega 2024, 9, 40122−40133

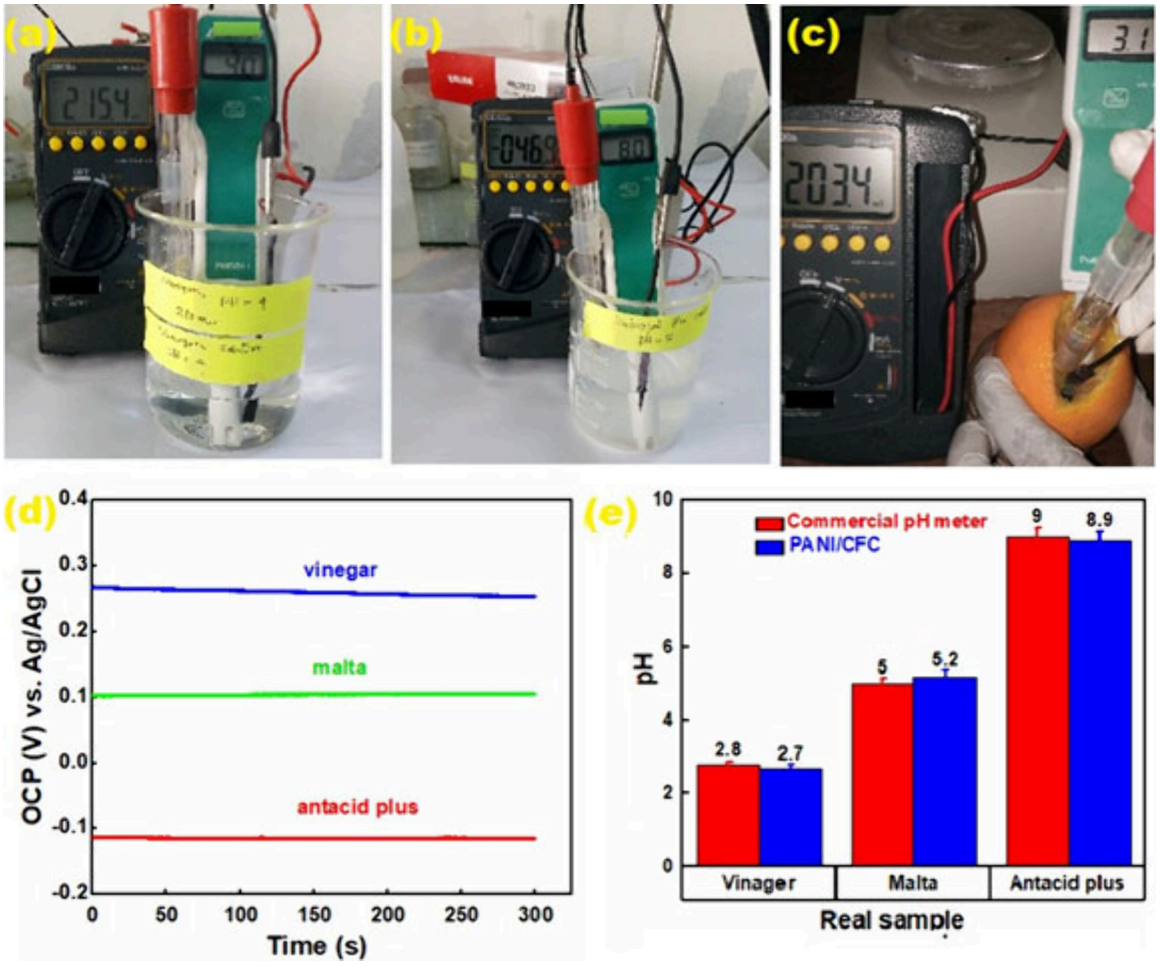

Figure 6. Real sample test images of (a) Vinegar solution; (b) the antacid plus; (c) Malta, (PANI-CFC working electrode and Ag/AgCl reference electrode); (d) OCP measurement of Malta, vinegar, and the antacid plus (conditions: PANI-CFC working electrode, platinum wire counter electrode, and Ag/AgCl reference electrode; 20 mL of each sample was taken for the measurement); and (e) Column representation of the comparison between PANI-CFC sensor and commercial pH meter.

measured pH values of 2.5 for Malta, 5.0 for vinegar, and 9.0 for the antacid solution (Figure 6e). These results demonstrate that the PANI-CFC sensor provides accurate and reliable pH measurements that are very close to those obtained with a commercial pH meter, validating the effectiveness of the PANI-CFC sensor for real-world pH measurement applications (Supplementary Figure S6).

3.11. Optimized Geometry and Interaction Energy Calculation Using DFT. The pH sensitivity of the sensor is associated with electrochemically deposited polyaniline on the carbon fiber cloth; therefore, we limit our theoretical investigation to the PANI-H^+ interaction. In doing so, polyaniline (Emeraldine base) oligomers (O-PANI) containing four repeating units of PANI (Supplementary Figure S7) and O-PANI-$2H^+$ structures were optimized at the DFT-B3LYP/6-311+G (d, p) level of theory (Supplementary Table S2). Geometrical parameters including bond lengths, bond angles, and dihedral angles are presented in Supplementary Table S3 which shows valuable insights on H^+ interaction with O-PANI. Bond length and bond angle variations were seen when two protons were added to O-PANI at N46 and N47, pointing to good sensitivity toward H^+. Additionally, the increase in dihedral angles (Supplementary Table S2) following protonation suggests an increase in coplanarity that facilitates the easy electron transfer from polyaniline to protons. We have also evaluated the interaction energy between this O-PANI and H^+ using eq 2 and the values are presented in Supplementary Table S1.

$$\Delta E_{int} = E_{reactant1} + E_{reactant2} - E_{product} \quad (2)$$

A large interaction energy of −173.2886 kcal/mol for O-PANI-$2H^+$ also indicates the sensitivity of this polymer sensor toward H^+. The amount of charge transfers between the O-PANI (sensors) and H^+ is simulated at the B3LYP/6-311G+ (d, p) level of theory to evaluate the change in electronic properties.[65,66] Mulliken charge analysis of isolated and proton bound O-PANI complexes are presented in Supplementary Table S4 and Supplementary Figure S8(a,b).

The total charge on a ring is calculated as the sum of charges found on all six carbons of the ring and directly attached hydrogen atoms. These rings have been designated as 1, 2, 3, and 4 in Supplementary Figure S7(a,b). Additionally, Supplementary Figure S8(a,b) shows a color change from read to green that denotes the relative negative to positive charges on the atoms. Charges of phenyl rings in O-PANI was observed 0.34(1) e^-, 0.588(2) e^-, 0.495(3) e^-, and 0.467 (4) e^- by Mulliken charge analysis. Upon protonation, rings charges reduced to 0.361(1) e^-, 0.347(2) e^-, 0.247(3) e^-, and 0.033(4) e^- respectively.

https://doi.org/10.1021/acsomega.4c06090
ACS Omega 2024, 9, 40122−40133

Based on Mulliken charge analysis, Nitrogen N46 in the O-PANI-2H$^+$ complex loses about 0.2 e$^-$ charge upon proton addition as H$^+$ transfers positive charge to the polymer backbone. In vibrational spectra of the 4PANI-H$^+$ complex, a few extra peaks have been seen which are absent for 4PANI (Supplementary Figure S9). On the grounds of quantum mechanics, the interaction between two interacting species takes place when the frontier molecular orbitals interact with each other. The magnitude of the change occurring in the energy difference of HOMO and LUMO as a result of interaction can explain the type and nature of bonding or interaction between sensor and analyte molecules (Figure 7).

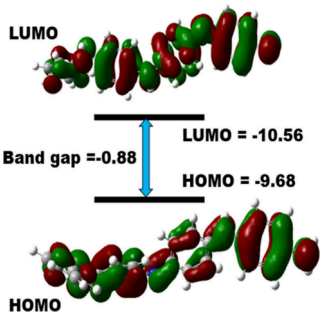

Figure 7. Frontier orbitals of protonated PANI and DFT B3LYP/6-311G+(d, p) level of theory.

The reactivity of a chemical species is also related to the energy of its HOMO. The higher the energy associated with HOMO, the greater will be its reactivity and *vice versa*.[67] The decrease in the energy of HOMO of a chemical species is the measure of the stability it attains as a result of a certain interaction. Calculations showed that on protonated with H$^+$, the energy of HOMO is decreased which indicates high stability of this protonated PANI. Supplementary Table S4 represents band gaps in terms of differences of HOMO and LUMO of deprotonated and protonated PANI.

Energies of HOMO and LUMO (EHOMO and ELUMO) of deprotonated 4PANI sensor (Supplementary Figure S10), as well as protonated PANI (4PANI-2H$^{+)}$ along with the variation in energy difference brought about in HOMO (ΔEHOMO) by protonated, are included in Table S5 and Supplementary Figure S10. The electrical conductivity of a chemical species can be related to the difference in energies of HOMO and LUMO or the HOMO−LUMO (H-L) gap or bandgap. Therefore, it is obvious that intramolecular charge transfer has predominantly happened during the excitation of the molecules. The computed energies of HOMO and LUMO are −4.80 eV and −2.2 eV for deprotonated PANI, − 10.56 eV and −9.68 eV for protonated PANI respectively. The magnitude of this H-L gap is inversely proportional to the electronic conductivity. The H-L gap in electron volts is given in Supplementary Table S4 for 4PANI, and 4PANI-2H$^+$. The magnitude of the H-L gap decreased greatly of protonated PANI prominently on sensing H$^+$, which was seen in Supplementary Table S5. The large decrease in band gap leads to the increase in electrical conductivity of the polymer on sensing H$^+$, which again confirms the selectivity of the polyaniline sensor toward H$^+$. Moreover, the contour structure of protonated peptides is shown in Figure 8.

4. CONCLUSIONS

In this work, a flexible pH sensor is developed based on electropolymerized polyaniline modified carbon fiber cloth as the sensing material. The PANI-CFC pH sensor was characterized using FESEM, XRD, FTIR, Raman spectroscopy, and XPS. The electrochemical properties of the pH sensor were characterized in terms of sensitivity, response time, repeatability, and stability. The sensor demonstrated a sensitivity of 60.9 mV/pH, which is close to the theoretical value predicted by the Nernstian behavior. In addition, the pH sensor exhibited excellent response times, repeatability, and stability. The pH values measured by the PANI-CFC sensor for real samples, such as vinegar, malta, and antacid, closely matched those obtained using a commercial pH meter.

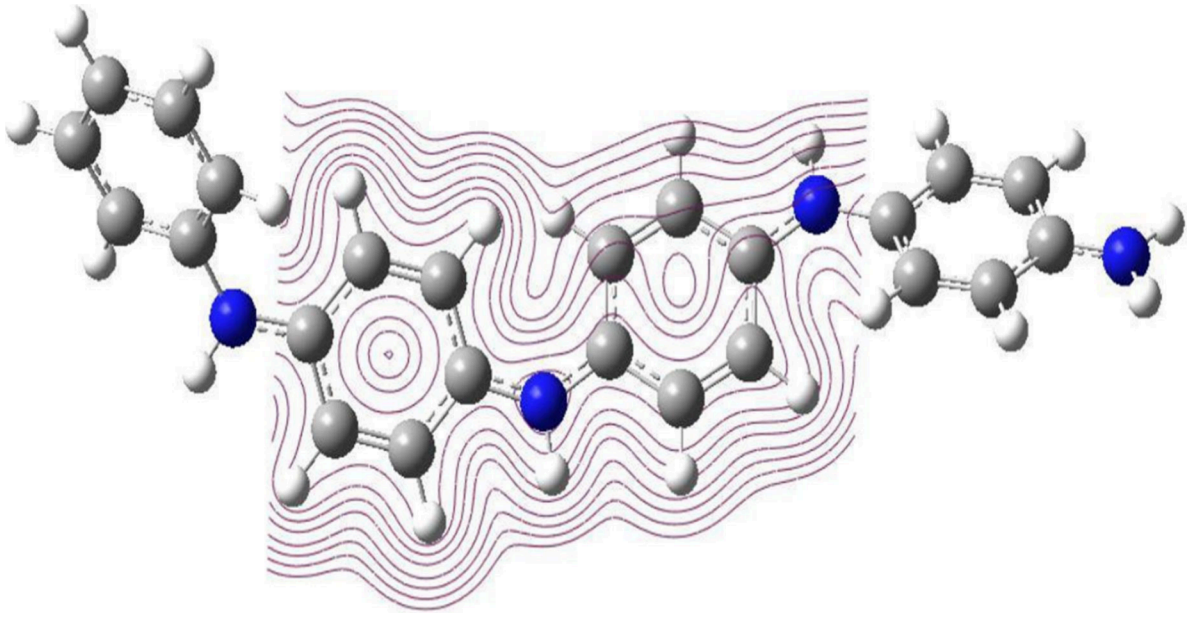

Figure 8. Contour structure of protonated PANI at the DFT B3LYP/6-311G+(2d,p) level of theory.

https://doi.org/10.1021/acsomega.4c06090
ACS Omega 2024, 9, 40122−40133

Importantly, the flexible pH sensor was capable of measuring pH changes on the curved surface of malta, an application that is not feasible by using conventional pH meters. This flexibility makes the sensor suitable for a wide range of applications including the food and pharmaceutical sector. Additionally, the effects of interfering ions and temperature were studied, indicating no significant effect on the PANI-CFC pH sensor. DFT calculations confirmed the high sensitivity of the PANI conducting polymer sensor to H^+ ions. Changes in geometric parameters indicated strong interactions, with interaction energy values reaching −173.2886 kcal/mol for the $2H^+$ complex. Mulliken charge and molecular orbital analyses showed consistent charge transfer trends with the experimental data. New peaks and shifts in vibrational spectra upon interaction further validated the sensor's high sensitivity and selectivity for H^+ ions. The sensor exhibits deviations under highly acidic and basic conditions. In future work, we will address this issue and aim to apply this sensor for measuring pH in biological fluids.

■ ASSOCIATED CONTENT

Supporting Information

The Supporting Information is available free of charge at https://pubs.acs.org/doi/10.1021/acsomega.4c06090.

Experimental details: optimized geometry and interaction energy descriptions, and additional figures and tables as noted in the text (PDF)

■ AUTHOR INFORMATION

Corresponding Authors

Kafil M. Razeeb − *Micro-NanoSystems Centre, Tyndall National Institute, University College Cork, Cork T12 R5CP, Ireland;* orcid.org/0000-0001-9360-9277; Email: kafil.mahmood@tyndall.ie

Mamun Jamal − *Department of Chemistry, Khulna University of Engineering & Technology, Khulna 9203, Bangladesh;* orcid.org/0000-0002-3617-7444; Email: mamun.jamal@chem.kuet.ac.bd

Authors

Md. Sanwar Hossain − *Department of Chemistry, Khulna University of Engineering & Technology, Khulna 9203, Bangladesh;* Present Address: Institute of National Analytical Research and Service (INARS), Bangladesh Council of Scientific and Industrial Research (BCSIR), Dhanmondi, Dhaka 1205, Bangladesh; orcid.org/0009-0006-6191-6022

Narayanasamy Padmanathan − *Micro-NanoSystems Centre, Tyndall National Institute, University College Cork, Cork T12 R5CP, Ireland*

Md. Mizanur R. Badal − *Department of Chemistry, Khulna University of Engineering & Technology, Khulna 9203, Bangladesh;* orcid.org/0000-0002-4119-4337

Complete contact information is available at: https://pubs.acs.org/10.1021/acsomega.4c06090

Notes

The authors declare no competing financial interest.

■ ACKNOWLEDGMENTS

The authors are grateful to the Ministry of Science & Technology of Bangladesh (Special Allocation Programme 2021-22, Grant Number: 582-Phy-2021-22).

■ REFERENCES

(1) Shi, X. M.; Mei, L. P.; Zhang, N.; Zhao, W. W.; Xu, J. J.; Chen, H. Y. A Polymer Dots-Based Photoelectrochemical PH Sensor: Simplicity, High Sensitivity, and Broad-Range PH Measurement. *Anal. Chem.* **2018**, *90* (14), 8300−8303.

(2) Li, Y.; Mao, Y.; Xiao, C.; Xu, X.; Li, X. Flexible PH Sensor Based on a Conductive PANI Membrane for PH Monitoring. *RSC Adv.* **2020**, *10* (1), 21−28.

(3) Näreoja, T.; Deguchi, T.; Christ, S.; Peltomaa, R.; Prabhakar, N.; Fazeli, E.; Perälä, N.; Rosenholm, J. M.; Arppe, R.; Soukka, T.; et al. Ratiometric Sensing and Imaging of Intracellular PH Using Polyethylenimine-Coated Photon Upconversion Nanoprobes. *Anal. Chem.* **2017**, *89* (3), 1501−1508.

(4) Yue, S.; Sun, X.; Wang, N.; Wang, Y.; Wang, Y.; Xu, Z.; Chen, M.; Wang, J. SERS−Fluorescence Dual-Mode PH-Sensing Method Based on Janus Microparticles. *ACS Appl. Mater. Interfaces* **2017**, *9* (45), 39699−39707.

(5) Shi, X.-M.; Mei, L.-P.; Zhang, N.; Zhao, W.-W.; Xu, J.-J.; Chen, H.-Y. A Polymer Dots-Based Photoelectrochemical PH Sensor: Simplicity, High Sensitivity, and Broad-Range PH Measurement. *Anal. Chem.* **2018**, *90* (14), 8300−8303.

(6) Consolati, T.; Bolivar, J. M.; Petrasek, Z.; Berenguer, J.; Hidalgo, A.; Guisán, J. M.; Nidetzky, B. Biobased, Internally PH-Sensitive Materials: Immobilized Yellow Fluorescent Protein as an Optical Sensor for Spatiotemporal Mapping of PH inside Porous Matrices. *ACS Appl. Mater. Interfaces* **2018**, *10* (8), 6858−6868.

(7) Choi, S. J.; Savagatrup, S.; Kim, Y.; Lang, J. H.; Swager, T. M. Precision PH Sensor Based on WO3 Nanofiber-Polymer Composites and Differential Amplification. *ACS Sens.* **2019**, *4* (10), 2593−2598.

(8) Korostynska, O.; Arshak, K.; Gill, E.; Arshak, A. State Key Laboratory of Nonlinear Mechanics (LNM), Institute of Mechanics, Chinese Academy of Sciences, Beijing 100080, China. *Sensors* **2007**, *7*, 3027.

(9) Lowe, B. M.; Sun, K.; Zeimpekis, I.; Skylaris, C.-K.; Green, N. G. Field-Effect Sensors−from PH Sensing to Biosensing: Sensitivity Enhancement Using Streptavidin−Biotin as a Model System. *Analyst* **2017**, *142* (22), 4173−4200.

(10) Jamal, M.; Dey, T. K.; Nasrin, T.; Khosla, A.; Razeeb, K. M. nanostructured materials for sensing pH: Evolution, fabrication and challenges. *J. Electrochem. Soc.* **2022**, *169* (5), No. 057517.

(11) Parrilla, M.; Cuartero, M.; Crespo, G. A. Wearable Potentiometric Ion Sensors. *TrAC Trends Anal Chem.* **2019**, *110*, 303−320.

(12) Park, H. J.; Yoon, J. H.; Lee, K. G.; Choi, B. G. Potentiometric Performance of Flexible PH Sensor Based on Polyaniline Nanofiber Arrays. *Nano Converg* **2019**, DOI: 10.1186/s40580-019-0179-0.

(13) Khan, M. I.; Mukherjee, K.; Shoukat, R.; Dong, H. A Review on PH Sensitive Materials for Sensors and Detection Methods. *Microsyst. Technol.* **2017**, *23*, 4391.

(14) Graham, D.; Jaselskis, B.; Moore, C. Development of the Glass Electrode and the PH Response. *J. Chem. Educ.* **2013**, *90*, 345−351.

(15) Nussbaum, R.; Jeanneret, S.; Bakker, E. Increasing the Sensitivity of PH Glass Electrodes with Constant Potential Coulometry at Zero Current. *Anal. Chem.* **2024**, *96* (16), 6436−6443.

(16) Olthuis, W.; Robben, M. A. M.; Bergveld, P.; Bos, M.; van der Linden, W. E. PH Sensor Properties of Electrochemically Grown Iridium Oxide. *Sensors Actuators B Chem.* **1990**, *2* (4), 247−256.

(17) Marzouk, S. A. M.; Ufer, S.; Buck, R. P.; Johnson, T. A.; Dunlap, L. A.; Cascio, W. E. Electrodeposited Iridium Oxide PH Electrode for Measurement of Extracellular Myocardial Acidosis during Acute Ischemia. *Anal. Chem.* **1998**, *70* (23), 5054−5061.

(18) Jamal, M.; Razeeb, K. M.; Shao, H.; Islam, J.; Akhter, I.; Furukawa, H.; Khosla, A. Development of tungsten oxide nanoparticle

modified carbon fibre cloth as flexible pH sensor. *Sci. rep* **2019**, *9* (1), 4659.
(19) Devlin, L.; Jamal, M.; Razeeb, K. M. Novel pH sensor based on anthraquinone−ferrocene modified free standing gold nanowire array electrode. *Anal Meth* **2013**, *5* (4), 880−884.
(20) Fog, A.; Buck, R. P. Electronic Semiconducting Oxides as PH Sensors. *Sens & Actuat* **1984**, *5* (2), 137−146.
(21) Liao, Y. H.; Chou, J. C. Preparation and Characteristics of Ruthenium Dioxide for PH Array Sensors with Real-Time Measurement System. *Sens Actuat, B Chem.* **2008**, *128* (2), 603−612.
(22) Lefèvre, V. *Nanowires: Properties, Synthesis, and Applications*; Nova Science Publishers, 2012.
(23) Hossain, M. S.; Yasmin, S.; Kabir, M. H. Cost-Effective Synthesis of Magnetic Graphene Oxide Nanocomposite from Waste Battery for the Removal of Arsenic from Aqueous Solutions: Adsorption Mechanism with DFT Calculation. *J. Saudi Chem. Soc.* **2024**, *28* (3), No. 101873.
(24) Ghoneim, M. T.; Nguyen, A.; Dereje, N.; Huang, J.; Moore, G. C.; Murzynowski, P. J.; Dagdeviren, C. Recent Progress in Electrochemical pH-Sensing Materials and Configurations for Biomedical Applications. *Chem. Rev.* **2019**, *119* (8), 5248−5297.
(25) Zhu, X.; Sun, H.; Yu, B.; Xu, L.; Xiao, H.; Fu, Z.; Gao, T.; Yang, X. A Flexible PH Sensor Based on Polyaniline@oily Polyurethane/Polypropylene Spunbonded Nonwoven Fabric. *RSC Adv.* **2024**, *14* (8), 5627−5637.
(26) Kim, S. J.; Park, H. J.; Kim, G.; Kim, J.; Lee, K. G.; Choi, B. G. Hydrodynamics-Engineered Polyaniline Nanofibers on Graphene Nanosheets for High-Performance PH Sensors. *Mater. Today Commun.* **2024**, *39*, No. 109224.
(27) Wang, R.; Zhai, Q.; Zhao, Y.; An, T.; Gong, S.; Guo, Z.; Shi, Q. Q.; Yong, Z.; Cheng, W. Stretchable Gold Fiber-Based Wearable Electrochemical Sensor toward PH Monitoring. *J. Mater. Chem. B* **2020**, *8* (16), 3655−3660.
(28) Yoon, J. H.; Kim, K. H.; Bae, N. H.; Sim, G. S.; Oh, Y.-J.; Lee, S. J.; Lee, T. J.; Lee, K. G.; Choi, B. G. Fabrication of Newspaper-Based Potentiometric Platforms for Flexible and Disposable Ion Sensors. *J. Colloid Interface Sci.* **2017**, *508*, 167−173.
(29) Mahinnezhad, S.; Izquierdo, R.; Shih, A. Fully Printed PH Sensor Based on Polyaniline/Graphite Nanocomposites. *J. Electrochem. Soc.* **2023**, *170* (2), No. 027501.
(30) Zhao, Y.; Guo, X.; Sun, H.; Tao, L. Recent Advances in Flexible Wearable Technology: From Textile Fibers to Devices. *Chem. Rec* **2024**, *24*, No. e202300361.
(31) Jian, M.; Wang, C.; Wang, Q.; Wang, H.; Xia, K.; Yin, Z.; Zhang, M.; Liang, X.; Zhang, Y. Advanced Carbon Materials for Flexible and Wearable Sensors. *Sci. China Mater.* **2017**, *60*, 1026.
(32) Ouyang, T.; Cheng, K.; Yang, F.; Jiang, J.; Yan, J.; Zhu, K.; Ye, K.; Wang, G.; Zhou, L.; Cao, D. A General In-Situ Etching and Synchronous Heteroatom Doping Strategy to Boost the Capacitive Performance of Commercial Carbon Fiber Cloth. *Chem. Eng. J.* **2018**, *335*, 638−646.
(33) Yoon, Y.; Truong, P. L.; Lee, D.; Ko, S. H. Metal-Oxide Nanomaterials Synthesis and Applications in Flexible and Wearable Sensors. *ACS Nanosci Au* **2022**, *2* (2), 64−92.
(34) Huerta, F.; Quijada, C.; Montilla, F.; Morallón, E. Revisiting the Redox Transitions of Polyaniline. Semiquantitative Interpretation of Electrochemically Induced IR Bands. *J. Electroanal. Chem.* **2021**, *897*, No. 115593.
(35) Santos, C. da C.; Pimenta, T. C.; Thomasini, R. L.; Verly, R. M.; Franco, D. L.; Ferreira, L. F. Electropolymerization of Phenol and Aniline Derivatives: Synthesis, Characterization and Application as Electrochemical Transducers. *J. Electroanal. Chem.* **2019**, *846*, No. 113163.
(36) Deshkulkarni, B.; Viannie, L. R.; Ganachari, S. V.; Banapurmath, N. R.; Shettar, A. Humidity Sensing Using Polyaniline/Polyvinyl Alcohol Nanocomposite Blend. *IOP Conf. Ser. Mater. Sci. Eng.* **2018**, *376* (1), 012063.
(37) Hussein, M. A.; Khan, A.; Alamry, K. A. A highly efficient electrochemical sensor containing polyaniline/cerium oxide nanocomposites for hydrogen peroxide detection. *RSC Adv.* **2022**, *12* (49), 31506−31517.
(38) Heineman, W. R. Polymer Film Chemically Modified Electrode as a Potentiometric Sensor. *Anal. Chem.* **1980**, *52* (2), 347−348.
(39) Cherchour, N.; Deslouis, C.; Messaoudi, B.; Pailleret, A. PH Sensing in Aqueous Solutions Using a MnO2 Thin Film Electrodeposited on a Glassy Carbon Electrode. *Electrochim. Acta* **2011**, *56* (27), 9746−9755.
(40) Gläb, S.; Hulanicki, A.; Edwall, G.; Folke, F.; Ingman, I.; Koch, W. F. Metal-Metal Oxide and Metal Oxide Electrodes as PH Sensors. *Crit. Rev. Anal Chem.* **1989**, *21* (1), 29−47.
(41) Shakoor, A.; Rizvi, T. Z.; Nawaz, A. Raman Spectroscopy and AC Conductivity of Polyaniline Montmorillonite (PANI − MMT) Nanocomposites. *J. Mater. Sci: Mater. Electron* **2011**, *22*, 1076−1080.
(42) Yu, P.; Li, Y.; Yu, X.; Zhao, X.; Wu, L.; Zhang, Q. Polyaniline Nanowire Arrays Aligned on Nitrogen-Doped Carbon Fabric for High-Performance Flexible Supercapacitors. *Langmuir* **2013**, *29* (38), 12051−12058.
(43) Morávková, Z.; Bober, P. Writing in a Polyaniline Film with Laser Beam and Stability of the Record: A Raman Spectroscopy Study. *Int. J. Polym. Sci.* **2018**, *2018* (1), No. 1797216.
(44) Howli, P.; Das, S.; Sarkar, S.; Samanta, M.; Panigrahi, K.; Das, N. S.; Chattopadhyay, K. KCo_3O_4 Nanowires on Flexible Carbon Fabric as a Binder-Free Electrode for All Solid-State Symmetric Supercapacitor. *ACS Omega* **2017**, *2* (8), 4216−4226.
(45) Pouget, J. P.; Józefowicz, M. E.; Epstein, A. J.; Tang, X.; MacDiarmid, A. G. X-Ray Structure of Polyaniline. *Macromolecules* **1991**, *24* (3), 779−789.
(46) Diggikar, R. S.; Deshmukh, S. P.; Thopate, T. S.; Kshirsagar, S. R. Performance of Polyaniline Nanofibers (PANI NFs) as PANI NFs-Silver (Ag) Nanocomposites (NCs) for Energy Storage and Antibacterial Applications. *ACS Omega* **2019**, *4* (3), 5741−5749.
(47) He, X.; Gao, B.; Wang, G.; Wei, J.; Zhao, C. A New Nanocomposite: Carbon Cloth Based Polyaniline for Anelectrochemical Supercapacitor. *Electrochim. Acta* **2013**, *111*, 210−215.
(48) Yasmin, S.; Kabir, M. H.; Shaikh, M. A. A.; Jeon, S. Electrochemically Reduced Graphene Oxide Supported Palladium-Cobalt Alloy Nanoparticles as Highly Efficient Electrocatalyst for Oxygen Reduction Reaction. *ECS J. Solid State Sci. Technol.* **2023**, *12* (11), No. 111004.
(49) Yasmin, S.; Roy, N.; Kabir, M. H.; Jeon, S. Electrochemically Reduced Graphene-Oxide Supported Bimetallic Nanoparticles Highly Efficient for Oxygen Reduction Reaction with Excellent Methanol Tolerance. *Appl. Surf. Sci.* **2022**, *9* (2), No. 100235.
(50) Yasmin, S.; Ahmed, D.; Park, S.; Jeon, S. Nitrogen-Doped Graphene Supported Cobalt Oxide for Sensitive Determination of Dopamine in Presence of High Level Ascorbic Acid. *J. Electrochem. Soc.* **2016**, *163*, B491.
(51) Yasmin, S.; Shamsuddin Ahmed, M.; Jeon, S. A Noble Silver Nanoflower on Nitrogen Doped Carbon Nanotube for Enhanced Oxygen Reduction Reaction. *Int. J. Hydrog Energy* **2017**, *42*, 1075.
(52) Yasmin, S.; Joo, Y.; Jeon, S. 2,3-Diaminopyridine Functionalized Reduced Graphene Oxide-Supported Palladium Nanoparticles with High Activity for Electrocatalytic Oxygen Reduction Reaction. *Appl. Surf. Sci.* **2017**, *406*, 226.
(53) Upoma, B. P.; Yasmin, S.; Shaikh, A. A.; Jahan, T.; Haque, A.; Moniruzzaman, M.; Kabir, H. A Fast Adsorption of Azithromycin on Waste-Product-Derived Graphene Oxide Induced by H - Bonding and Electrostatic Interactions. *ACS Omega* **2022**, *7* (34), 29655−29665.
(54) Roy, N.; Yasmin, S.; Jeon, S. Effective Electrochemical Detection of Dopamine with Highly Active Molybdenum Oxide Nanoparticles Decorated on 2, 6 Diaminopyridine/Reduced Graphene Oxide. *Microchem J.* **2020**, *153*, No. 104501.
(55) Yasmin, S.; Ahmed, M. S.; Park, D.; Jeon, S. Nitrogen-Doped Graphene Supported Cobalt Oxide for Sensitive Determination of Dopamine in Presence of High Level Ascorbic Acid. *J. Electrochem. Soc.* **2016**, *163* (9), B491−B498.
(56) Liu, S.; Wen, B.; Jiang, X.; Waterhouse, G. I. N.; Zhang, Z. M.; Yu, L. M. Enhanced Photocathodic Antifouling/Antibacterial Proper-

https://doi.org/10.1021/acsomega.4c06090
ACS Omega 2024, 9, 40122−40133

ties of Polyaniline−Ag−N-Doped TiO2 Coatings. *J. Mater. Sci.* **2020**, *55* (34), 16255−16272.
(57) Maruthapandi, M.; Saravanan, A.; Luong, J. H. T.; Gedanken, A. Antimicrobial Properties of the Polyaniline Composites against Pseudomonas Aeruginosa and Klebsiella Pneumoniae. *J. Funct. Biomater.* **2020**, *11* (3), 59.
(58) Yasmin, S.; Ahmed, M. S.; Jeon, S. Determination of Dopamine by Dual Doped Graphene-Fe2O3 in Presence of Ascorbic Acid. *J. Electrochem. Soc.* **2015**, *162*, B363.
(59) Yasmin, S.; Kabir, M. H.; Roy, N.; Jeon, S. S. Nitrogen-Functionalized Carbon Nanotube Based Palladium Nanoparticles as an Efficient Catalyst for Oxygen Reduction and Ethanol Oxidation Reaction. *Appl. Surf. Sci.* **2022**, *9* (2), No. 100235.
(60) Perumal, A.; Kanumuri, R.; Rayala, S. K.; Nallaiyan, R. Fabrication of Bioactive Corrosion-Resistant Polyaniline/TiO_2 Nanotubes Nanocomposite and Their Application in Orthopedics. *J. Mater. Sci.* **2020**, *55* (32), 15602−15620.
(61) Azam, M. G.; Kabir, M. H.; Shaikh, M. A. A.; Ahmed, S.; Mahmud, M.; Yasmin, S. A Rapid and Efficient Adsorptive Removal of Lead from Water Using Graphene Oxide Prepared from Waste Dry Cell Battery. *J. Water Process Eng.* **2022**, *46*, No. 102597.
(62) Yasmin, S.; Kabir, M. H.; Roy, N.; Jeon, S. The Effect of Reducing Agent for Synthesizing Palladium Nanoparticle on Carbon Nanotube Support and Its Superior Catalytic Activity towards Methanol Oxidation Reaction. *ECS Adv.* **2023**, *2* (2), No. 024504.
(63) Zhao, Y.; Yu, Y.; Zhao, S.; Zhu, R.; Zhao, J.; Cui, G. Highly Sensitive PH Sensor Based on Flexible Polyaniline Matrix for Synchronal Sweat Monitoring. *Microchem J.* **2023**, *185*, No. 108092.
(64) Zea, M.; Texidó, R.; Villa, R.; Borrós, S.; Gabriel, G. Specially Designed Polyaniline/Polypyrrole Ink for a Fully Printed Highly Sensitive PH Microsensor. *ACS Appl. Mater. Interfaces* **2021**, *13* (28), 33524−33535.
(65) Ullah, H.; Shah, A. U. H. A.; Bilal, S.; Ayub, K. DFT Study of Polyaniline NH3, CO2, and CO Gas Sensors: Comparison with Recent Experimental Data. *J. Phys. Chem. C* **2013**, *117* (45), 23701−23711.
(66) Farooqi, B. A.; Yar, M.; Ashraf, A.; Farooq, U.; Ayub, K. Polyaniline Emeraldine Salt as Selective Electrochemical Sensor for HBr over HCl: A Systematic Density Functional Theory Study through Oligomer Approach. *J. Mol. Model* **2020**, *26*, 1−12.
(67) Kumar, A.; Srivastava, A. K.; Gangwar, S.; Misra, N.; Mondal, A.; Brahmachari, G. Combined Experimental (FT-IR, UV-Visible Spectra, NMR) and Theoretical Studies on the Molecular Structure, Vibrational Spectra, HOMO, LUMO, MESP Surfaces, Reactivity Descriptor and Molecular Docking of Phomarin. *J. Mol. Struct.* **2015**, *1096*, 94−101.

https://doi.org/10.1021/acsomega.4c06090
ACS Omega 2024, 9, 40122−40133